Inter-conversion of chemiosmotic parameters and its inhibition in *Thiobacillus ferrooxidans*

Niladri S. Kar, Tapas Kr. Datta and Anjan Kr. Dasgupta

Department of Biochemistry and Biophysics, University of Kalyani, Kalyani, Nadia 741 235, India.

In *Thiobacillus ferrooxidans*, an iron oxidizing obligatory acidophilic bacterium, bioenergetics was found to be critically dependent on sulphate distribution across its membrane. Under physiological condition, the sulphate distribution was found to be far from its electrochemical equilibrium, and a high residual proton motive force (~110 mV) remained conserved under varying external pH even in respiration-starved cells. The inter-conversion between bioenergetic parameters, namely membrane potential and pH gradient, was inhibited at a critical, low pH. Below this critical pH, proton-coupled sulphate influx was observed, as measured by radio-labelled transport assay, leading to collapse of the two chemiosmotic gradients. The associated alteration of membrane structure and permeability property was monitored by intrinsic fluorescence of *T. ferrooxidans* and extrinsic fluorescent probes.

ACIDOPHILIC bacteria have the remarkable ability to maintain their cytoplasmic pH close to neutrality even when external pH is below 4 (refs 1, 2). These cells, thus, can be taken as model system of chemiosmotic theory *in extremis*. According to this theory, the primary free energy available to a cell is its proton motive force (PMF)[3], which is composed of two parameters, namely the chemical gradient and the electrical gradient of proton:

$$\Delta p = 60\ \Delta\text{pH} - \Delta\psi, \qquad (1)$$

where $\Delta\psi$ and ΔpH are membrane potential and pH gradient across the energy-transducing membrane, respectively. Obviously, chemiosmotic theory demands a mechanism of inter-conversion between these two parameters so that PMF can be kept constant. Moreover, since cytoplasmic pH is fairly conserved, the membrane potential varies under different physiological conditions. Most of the acidophiles, including *T. ferrooxidans*, are reported to have inside positive $\Delta\psi$; generation of membrane potential is observed in the presence of protonophores or in respiration-inhibited cells[4–8]. The respiratory chain of *T. ferrooxidans* utilizes oxidation of Fe^{2+} to Fe^{3+}, and therefore, the available free energy is so small that cytochrome oxidase cannot pump protons from the cytoplasm to the external medium[9,10]. Thus, an efficient mechanism for respiration-independent ΔpH–$\Delta\psi$ inter-conversion may be present in this organism, which is yet to be reported explicitly.

The initial objective of this work was to detect physiological limits of the interconvertibility of the two bioenergetic parameters. Our preliminary observation indicates that there exists a critical external pH, at which the inter-conversion fails[11]. The mechanism of such failure may provide important insights towards better understanding of bioenergetic regulation in *T. ferrooxidans*.

T. ferrooxidans (ATCC 23270) was grown in 9 K medium[12] at pH 2.0 with aeration. Cells were harvested by centrifugation at 10,000 *g* for 15 min at 25°C, washed in ferrous free 9 K medium (9 K$^-$) and 10 mM sulphuric acid (pH 2.0), filtered through a Whatman No. 1 paper and remaining trace of iron precipitate was removed by centrifugation on silicone oil (high density, $\rho = 1.050$) at 1,000 *g* for 3 min.

Membrane potential and internal pH were determined by using $S^{14}CN^-$ and [^{14}C]acetate by rapid centrifugation method[4,13]. For measurement of membrane potential, cells at protein concentration of about 5 mg/ml were incubated with ^3H_2O (5 µCi/ml) and $KS^{14}CN$ (0.2 µCi/ml). For pH gradient, Na-[^{14}C]acetate (0.2 µCi/ml) or [^{14}C]chloroacetate (0.2 µCi/ml) were used. After duel incubation with ^3H_2O and the probe for membrane potential or pH gradient for 5 min at room temperature, the cells were separated by rapid centrifugation through dibutyl phthalate ($\rho = 1.043$) at 12,000 g for 5 min. The bacterial pellet was dissolved in 1% SDS, diluted in scintillation cocktail-W and counts were taken in a liquid scintillation counter (Model LS 5000 TD, Beckman). The membrane potential and pH gradient were calculated using the following equations:

$$\Delta\psi = 60 \log \{[\text{SCN}]_{in}/[\text{SCN}]_{out}\}, \qquad (2)$$

$$\Delta\text{pH} = \log \{[\text{A}]_{in}/[\text{A}]_{out}\,(1 + 10^{\text{pHout-pKa}})-1\} + \text{pK}_a\text{-pH}_{out}, \qquad (3)$$

where the subscripts 'in' and 'out' represent concentrations in the cytoplasm and the supernatant, respectively.

To measure internal buffering capacity of the whole cells and proton flux across their membrane, a procedure described previously[8] was followed. Cells permeabilized with 10% Triton X-100 were suspended in water at concentration 3.5 mg/ml. After each addition of acid pulse of 2.5–10 µl 20 m(N) HCl, pH was measured by an expandable ion analyser (Model EA920, Orion Research Inc., USA). 10% Triton X-100 and intact cells suspended in water were used as two controls. The value of the buffering capacity was expressed in nmole of proton required to change the pH by one unit per mg of cell protein. To measure proton flux across membrane, cells at 3.5 mg/ml were suspended in unbuffered assay medium (dilute H_2SO_4) and treated as required. pH was

monitored at intervals and proton influx was calculated from alkalization of the external medium[8].

Cells were suspended in 10 mM Tris-Cl (pH 7.0) containing 0.4 M sucrose and 20 mM EDTA and then treated with lysozyme at 0.2 mg/ml for 30 min. The reaction mixture was diluted with 0.4 M sucrose containing 10 mM $MgCl_2$. Swelling of the pre-formed spheroplasts was monitored by absorbance at 600 nm or by using ^3H_2O.

The fluorescence experiments were carried out in a Shimadzu RF-540 spectroflurometer at room temperature. Whole cells at 50 µg/ml were excited at 295 nm (2.5 nm slit) and the fluorescence spectra were recorded in the wavelength range 300–380 nm (2.5 nm slit). Quenching experiments were performed with excitation at 295 nm (slit 2 nm) and emission at 335 nm (slit 2–5) with increasing concentrations of quenchers: acrylamide 33.3–200 mM, copper sulphate 5–30 mM and potassium iodide 5–30 mM. Stern–Volmer constants were calculated from the slopes of $F0/F1$ vs $[Q]$ plots, where $F0$ and $F1$ were the unquenched and the quenched fluorescence intensities, respectively, and $[Q]$ was the quencher concentration[14].

The cells at 100 µg/ml were incubated with 10 µM of 8-anilino-1-naphthalene sulphonate (ANS) for 15 min and the fluorescence spectra were obtained with maximum intensity of excitation at 365 nm (2.5 nm slit) and emission wavelength range 400–550 nm (2.5 nm slit).

The cells without or with protonophore were incubated with [^{35}S]sulphuric acid. Then they were isolated by oil centrifugation and isotope distribution in the pellet and the supernatant was measured at different time intervals. To calculate internal concentration of sulphate, the internal volume was determined by ^3H_2O distribution.

The earlier reports on bioenergetics of *Thiobacilli* have claimed that maintenance of internal pH in the acidophiles is not an energy-dependent process[4,8]. In respiration-inhibited *T. ferrooxidans* and *T. acidophilus*, PMF of about 58 mV and 36 mV have been reported, while in the active cells the pmf values were 256 mV and 90 mV, respectively[4,5]. In both the cases cytoplasmic acidification was only by 0.4 pH unit. We report here existence of a protonophore-sensitive PMF and its conservation over a pH range in the non-respiring *T. ferrooxidans* cells. When *T. ferrooxidans* cells were incubated in $9K^-$ medium of pH 1.8 to pH 3.4, membrane potential and pH gradient were found to decrease with increasing external pH (Figure 1), with pmf remaining conserved at about 110 mV. When the external medium was replaced by β-alanine sulphate buffer of respective pH, the values of these parameters remained virtually the same. Over the pH range under study, therefore, the $\Delta\psi$–ΔpH inter-conversion is neither a respiration-dependent process nor dependent on alkalication uptake by the cells.

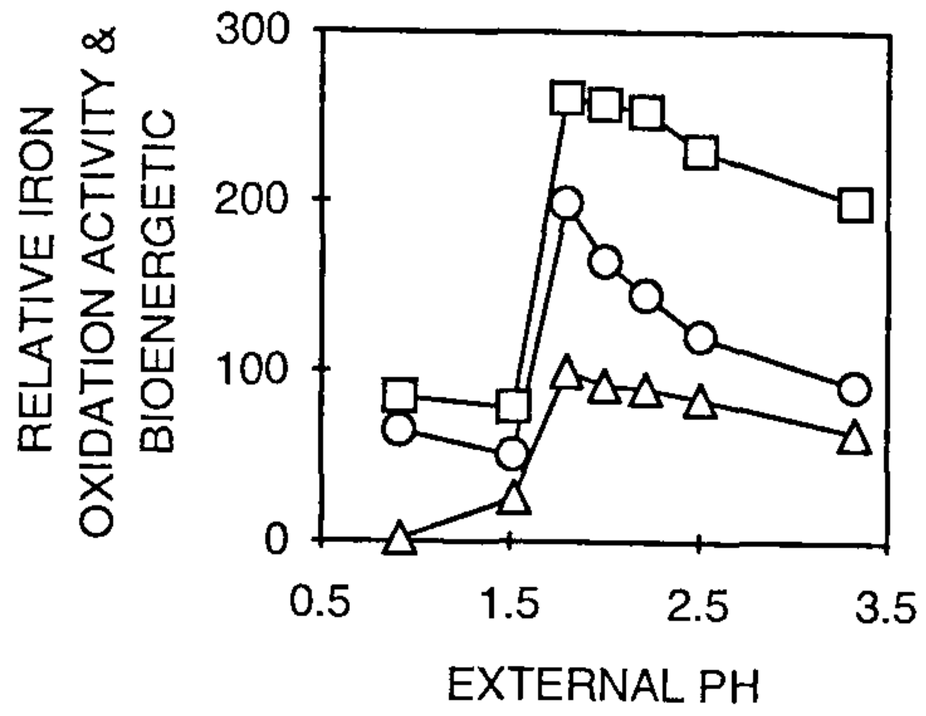

Figure 1. pH profiles of relative ferrous oxidation activity and bioenergetic parameters of *T. ferrooxidans*. Oxidation activity (Δ), membrane potential (O) and pH gradient (□) were measured in non-respiring condition as described in text. The cells were starved for about 6 h during their harvesting and purification.

As pointed out by several workers, the redox span (ΔE_h) between Fe^{2+}/Fe^{3+} ($E_{m,2} = 780$ mV) and H^+/H_2O ($E_{m,6.5} = 850$ mV) couples is only 70 mV and so in the respiring cells (where the membrane potential is small and PMF is high[4]), the electron transfer provides little scope for proton pump activity. However, this report indicates that the bioenergetics of the non-respiring cells might be qualitatively different. The large membrane potential that builds up in non-respiring cells is to be added to the redox span[15], giving a Gibbs free energy change per electron translocation:

$$\Delta G = -F\,(\Delta E_h + \Delta\psi), \qquad (4)$$

where F is the Faraday constant. Thus, respiration at pH 2.0 is expected to yield 22.7 kJ mol^{-1} in these cells compared to only 6.8 kJ mol^{-1} in the respiring cells. Though the implication of this is not yet clear, the generation of inside-positive membrane potential upon respiration deprivation appears to be thermodynamically beneficial, though perhaps transiently.

At very low pH (below pH 1.8), however, $\Delta\psi$ decreased discontinuously to a baseline at 65–70 mV. pH shift experiments indicated that after a brief exposure to such low pH, cells failed to regain high $\Delta\psi$ or to oxidize ferrous even when shifted to pH 2.0.

T. ferrooxidans showed typical pH dependence in its iron-oxidizing activity with a maximum near pH 2.0, its physiological pH (Figure 1). A comparison of the pH profile of iron oxidation and that of $\Delta\psi$ reveals remarkable similarity.

At pH 3.4 after treatment with 200 µM of 2,4-dinitrophenol (DNP), $\Delta\psi$ increased from 93 mV to 142 mV. These DNP-treated cells could respire as evident from ferrous oxidation after they were re-suspended at

pH 2.0. The value of cytoplasmic buffering capacity was found to be 95 nmole of proton per pH unit per mg of protein, while DNP-mediated proton influx was 65 nmole per mg of cell protein. Therefore, the cytoplasm should have been acidified by about 0.7 pH unit, which was exactly what was found by radio-isotopic measurement of pH gradient. Thus, though protonophore treatment gave rise to almost complete abolition of pmf, an appreciable ΔpH remained. The protonophore appears to introduce a proton influx that attains electrochemical equilibrium and becomes self-limiting in the absence of compensatory charge translocation[2,8]. Under this condition, internal buffering capacity could provide protection against internal acidification. This passive mechanism of pH homeostasis is therefore important even in the non-respiring cells where increasing amount of proton remains unabated in the cytoplasm due to non-functioning terminal oxidase. Since the proton influx was comparable with the amount of DNP in the assay medium (57 nmole/mg of cell protein), prevention of reverse flow of the 'uncoupler' by inside-positive membrane potential suggested earlier[16] seems to be operative.

Effect of protonophore treatment was, however, found to be external-pH dependent. At pH 1.8, for example, treatment with 200 µM of DNP resulted in abolition of pH gradient. The cells were unable to respire after DNP was washed away. Interestingly, the change in the other chemiosmotic parameter was anomalous – $\Delta\psi$ was found to decrease from 199 mV to 68 mV. Collapse of $\Delta\psi$ in presence of protonophore has been reported in at least another acidophile and interpreted as non-specific disruption of membrane at high DNP concentration[7].

Protonophore-induced collapse of the membrane potential, appreciable proton influx and inactivation of cells near pH 2 could only be accounted for by considering translocation of charges other than proton. Presumably, anion of assay medium could provide a compensatory conductance to proton influx under this condition.

Upon excitation at 275 nm or 295 nm, *T. ferrooxidans* cells showed an intrinsic fluorescence spectra with emission maximum at about 338 nm, presumably blue-shifted spectra of tryptophan (Trp) residues[14]. Comparison of relative intensity of intrinsic fluorescence of the membrane, its high-ionic strength removable and non-removable fractions, and cytoplasmic fraction showed the whole cell fluorescence was predominantly due to integral membrane protein[11]. When external pH was varied from 1.1 to 3.5, the fluorescence intensity was found to increase with increasing pH with no appreciable shift in wavelength maximum (Figure 2 *a*). Invariant emission maximum over the pH range indicates that the Trp residues were in a similar environment. Ionic collision quenchers of membrane-bound fluorophores have been used to monitor their accessibility to the fluorophore site[14,17]. Stern–Volmer plots for various quenchers of Trp were found to be linear, suggesting one class of fluorophores (Figure 3). Over the pH range of 1.1 to 3.5, the Stern–Volmer constants (K_{SV}) for acrylamide and Cu^{++} were 3.04 ± 0.18 M^{-1} and 9.17 ± 1.27 M^{-1}, respectively (Figure 3 *a* and *b*). For I^-, however, K_{SV} increased with decreasing pH, dramatically near pH 1.6 (Figure 3 *c*). Though K_{SV} of acrylamide and copper varied in narrow ranges, increase in the iodide-quenching constant at low pH suggests that the intrinsic fluorophores in the whole cells became more accessible to added anions.

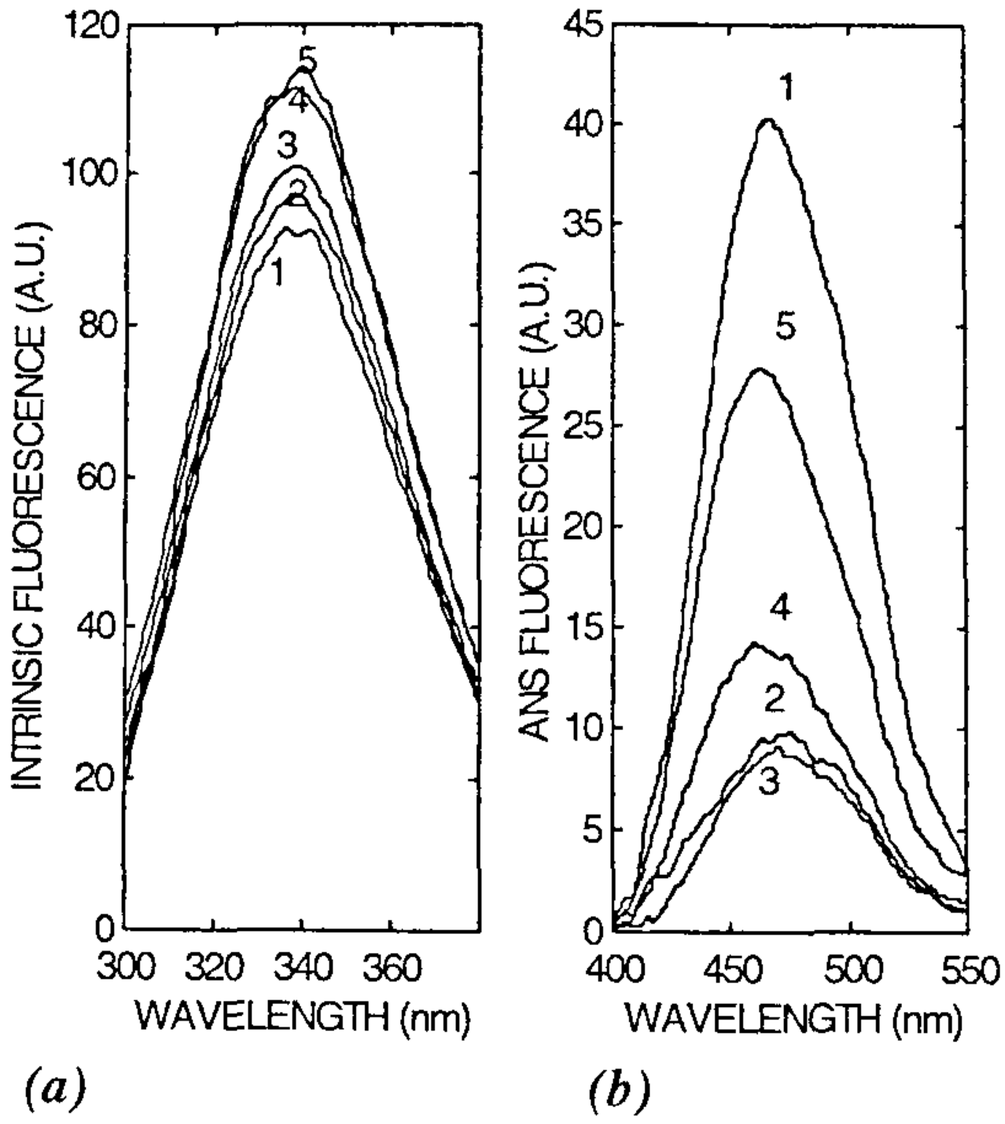

Figure 2. Emission spectra of intrinsic fluorescence (*a*) and ANS fluorescence (*b*). External pH values were pH 1.1 (1), pH 1.5 (2), pH 1.9 (3), pH 2.9 (4) and pH 3.5 (5). Each intrinsic fluorescence spectrum was corrected for background fluorescence of buffer, and each ANS spectrum (ANS concentration 10 µM) was corrected for buffer, free ANS and cells.

Binding studies of ANS have been used to determine fixed charges on the membrane surface[18]. The pH profile of ANS fluorescence intensity showed discontinuity between pH 1.5 and 1.9 (Figure 2 *b*). Below pH 1.4, slight red-shift in the emission spectra was also observed. The cells pre-incubated in such a low pH and then shifted to higher pH (i.e. pH 2.0) showed ANS spectrum similar to those suspended at the former pH. Thus, ANS fluorescence appears to monitor some irreversible alteration in the membrane structure at low pH.

Preliminary permeability study with spheroplasts showed osmotic swelling at higher concentrations of sulphate (Table 1), suggesting influx of sulphate and its counter-ion. The direct assay revealed a fast followed

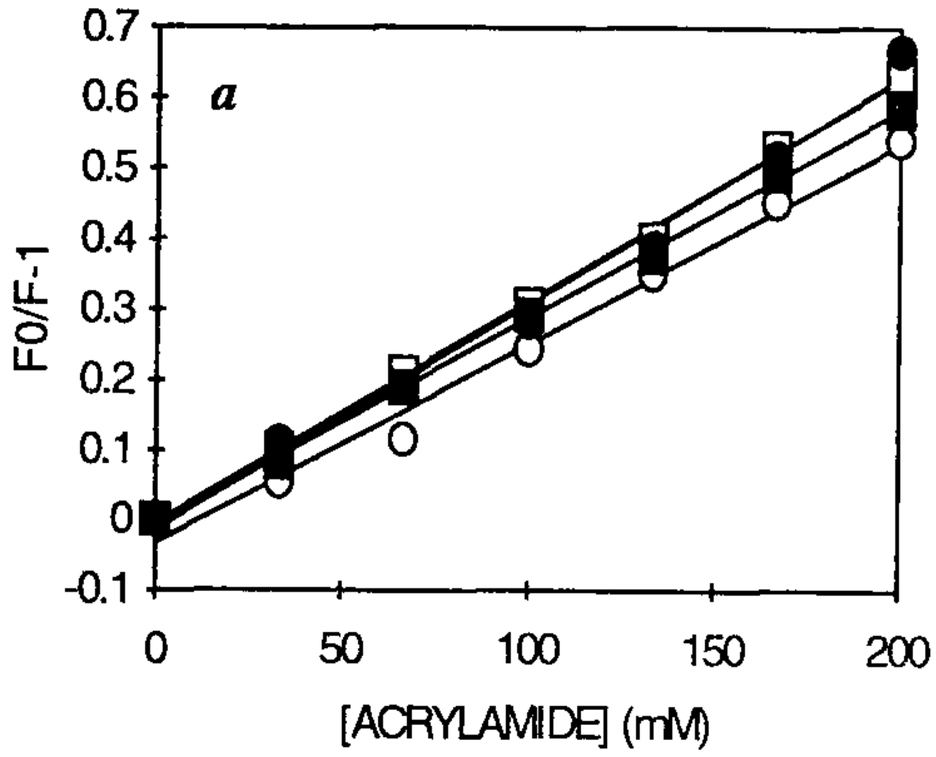

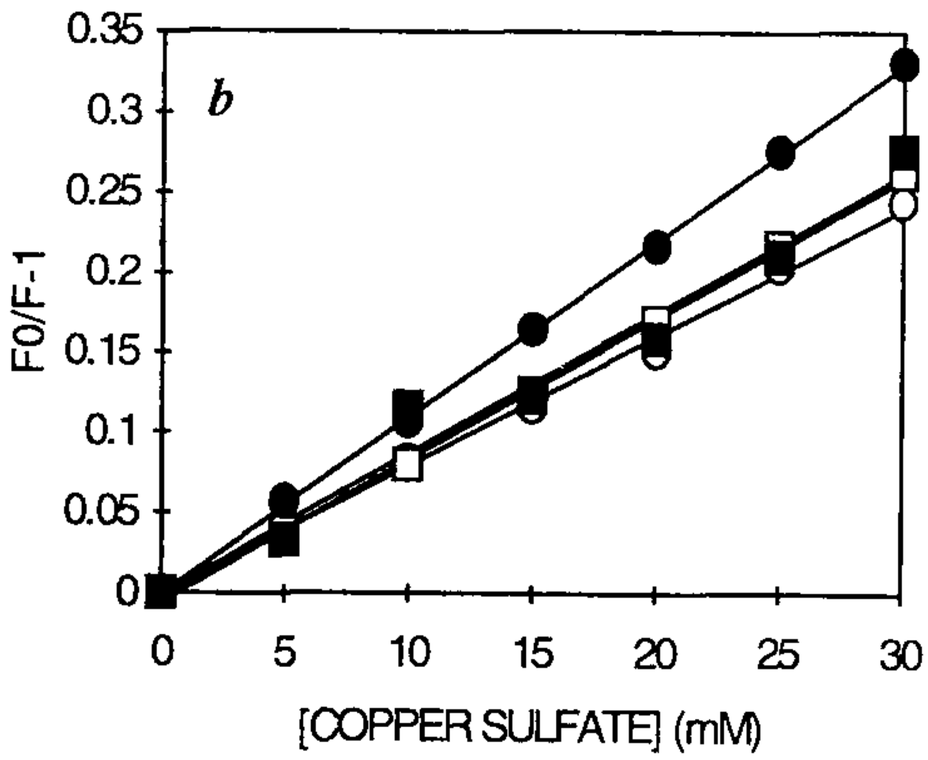

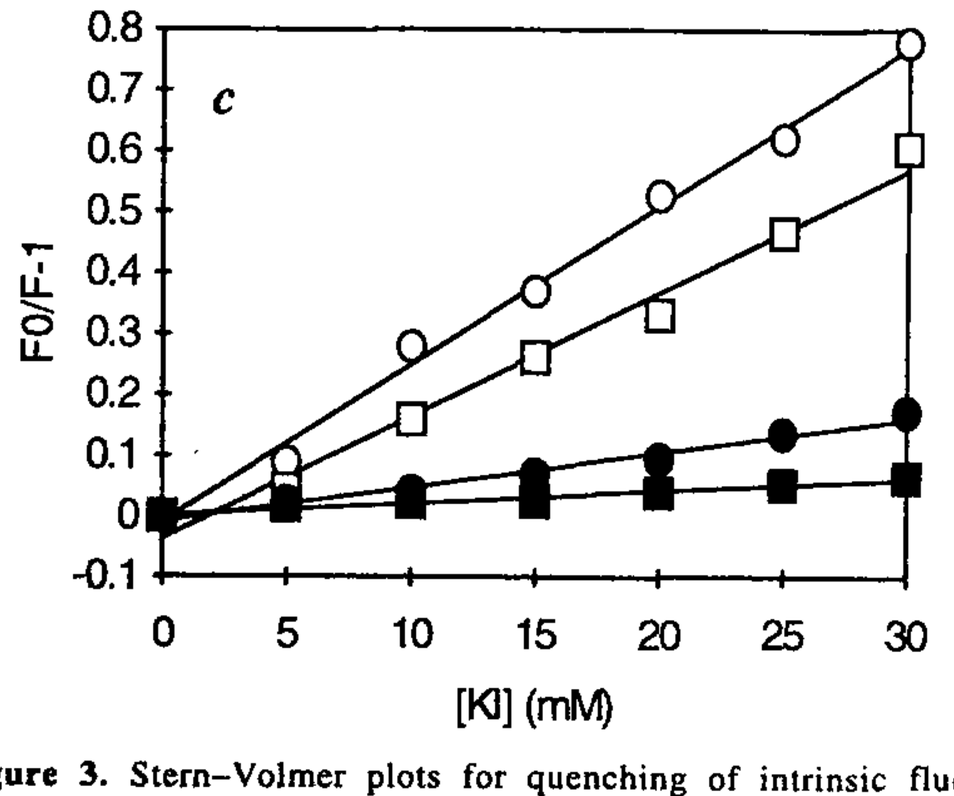

Figure 3. Stern–Volmer plots for quenching of intrinsic fluorescence with acrylamide (*a*), copper (*b*) and iodide (*c*). pH 1.4: (○); pH 1.6 (□); pH 1.9: (●); pH 3.3: (■). Linear correlation coefficients were greater than 0.995.

by a slow sulphate distribution in the cells (Figure 4). At pH 2.0, the sulphate concentration in DNP-treated cells was about twice as much as that in the control. This is in conformation with our observation regarding anomalous changes in the bioenergetic parameters and compensatory anionic charge movement. Assuming the

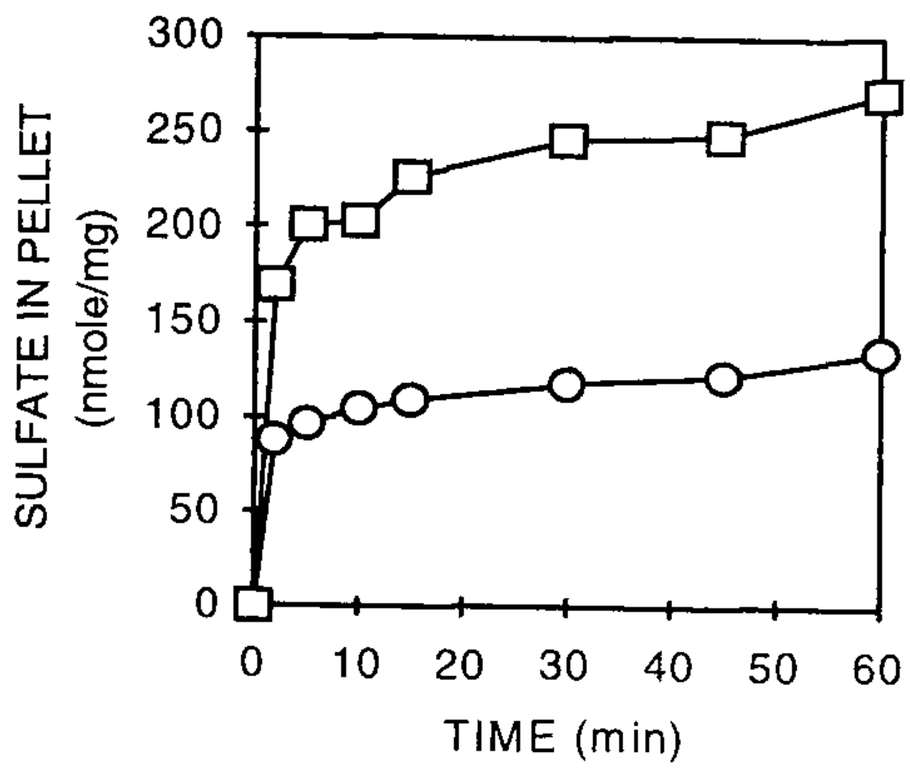

Figure 4. Time kinetics of sulphate accumulation. Cells suspended in $9K^-$ medium (pH 2.0) at protein concentration of 5 mg/ml were incubated without or with 200 μM DNP for 15 min and [^{35}S]sulphuric acid at final concentration of 0.05 μCi/ml was added to each tube at $t = 0$ min. Pellet counts of aliquots were taken at intervals. Control (○), DNP treated (□).

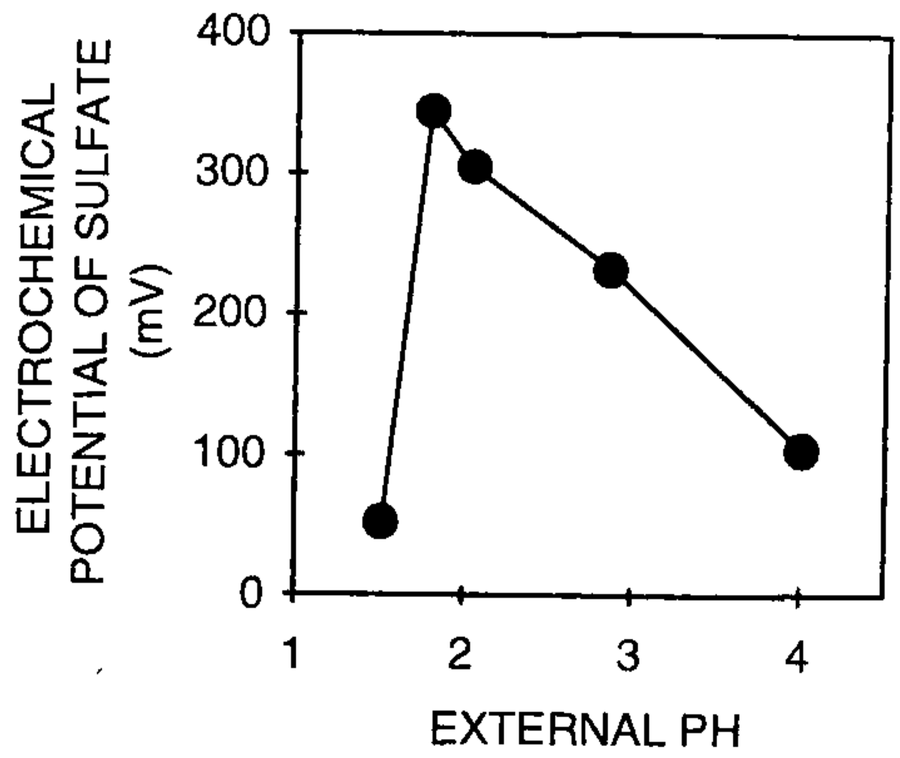

Figure 5. pH profile of the electrochemical potential of sulphate ion across the membrane. The parameter was measured from sulphate distribution ratio and membrane potential: $\Delta\mu_{SO4} = 2\Delta\psi - 60 \log ([SO_4]_{in}/[SO_4]_{out})$.

Table 1. Effect of sulphate on spheroplast swelling. For optical experiments, spheroplast preparation was suspended at protein concentration of 50 μg/ml and incubated for 5 min with increasing sulphate concentration. For direct measurement of volume, the spheroplasts were suspended at protein concentration of 7 mg/ml in various sulphate concentrations for 5 min and the volume was obtained with ^3H_2O

Sulphuric acid concentration (mM)	Absorbance at 600 nm	Volume (μl/mg of protein)
10	0.185 ± 0.01	3.05 ± 0.09
100	0.182 ± 0.02	3.21 ± 0.04
200	0.172 ± 0.02	3.80 ± 0.10

± indicates the standard deviations from mean values.

Nernst equilibrium distribution of SO_4^{-2}, the expected distribution ratios ($[SO_4]_{in}/[SO_4]_{out}$) are 3.2×10^5 and 54

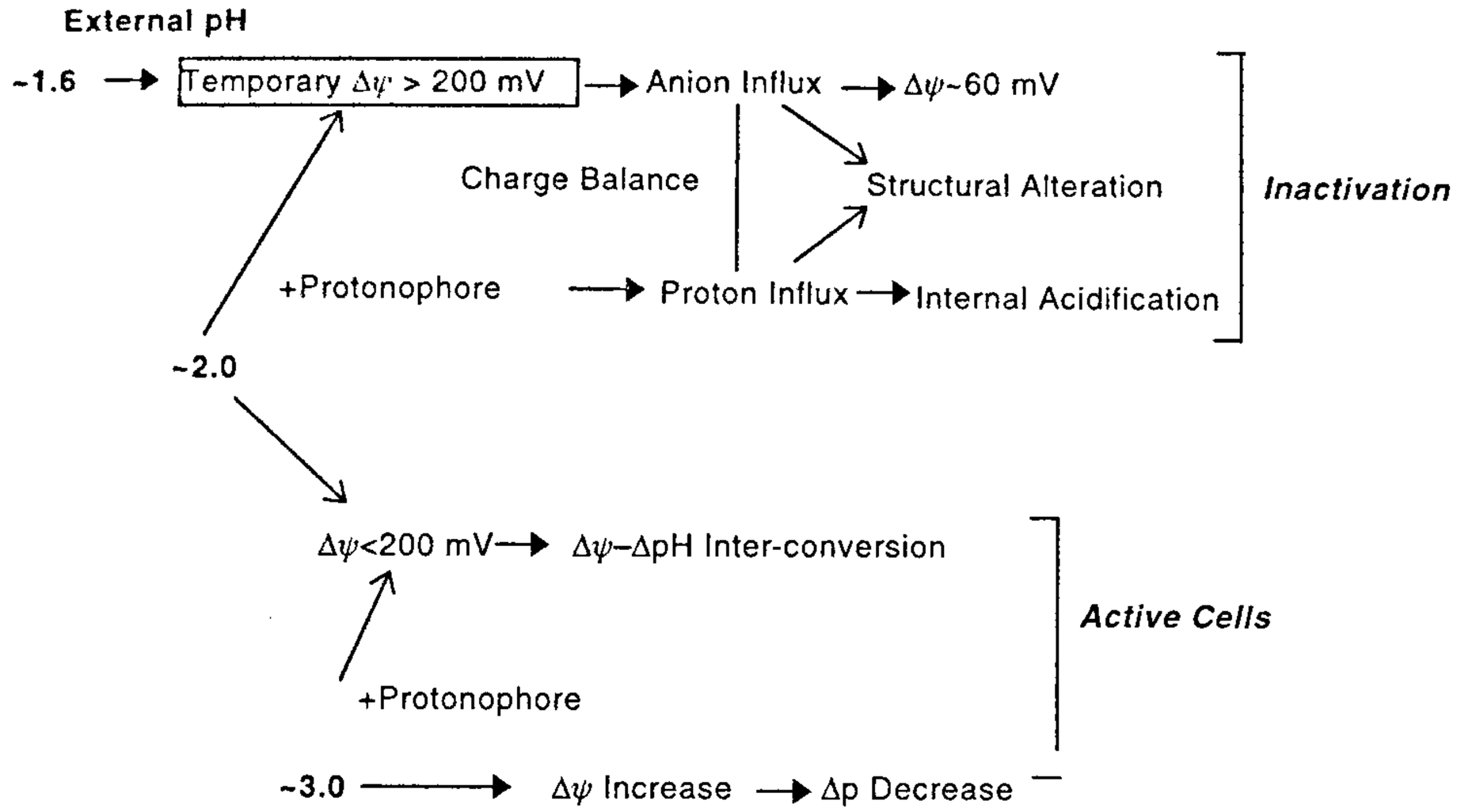

Figure 6. Scheme for relationship between bioenergetic parameters and ion uptake in *T. ferrooxidans*. Existence of a critical, high membrane potential has been proposed, above which the membrane breakdown phenomenon was observed.

at membrane potential of 165 and 52 mV, respectively. Thus, the sulphate ions are subjected to a high $\Delta\psi$ driven inward drag in the active cells, but not in the inactive cells.

The pH dependence of the electrochemical potential of sulphate ion is depicted in Figure 5. The critical pH induced increased sulphate permeability and consequently the sulphate electrochemical potential decreased toward the equilibrium. Inside-positive membrane potential in acidophiles may play some defensive role against cytoplasmic acidification and cation toxicity, but at the same time it may assist anion influx. In fact toxicity toward inorganic, monovalent anions in *T. ferrooxidans* has been shown to be due to their membrane-potential driven accumulation in the cytoplasm[19]. In *T. thiooxidans* protonated form of sulphite, sulphurous acid or sulphur dioxide has been reported to penetrate and acidify the cells[20]. However, sulphate ion, having an appreciable dipole moment even in its fully protonated form, is likely to be impermeable to lipid bilayer. This is in agreement with our observation that sulphate was effectively excluded from the active cells. In fact, the electrochemical gradient of sulphate was sufficient to maintain a PMF of 110 mV over the pH range 1.8–4.0 (Figure 5). It is tempting to assume that an electrogenic sulphate transport system, perhaps directly coupled to proton translocation, plays some crucial role in bioenergetics of *T. ferrooxidans*.

So far, only limited interpretation is available to explain the characteristic pH profile of iron oxidation by *T. ferrooxidans*. In this report, we propose a bioenergetic basis of its discontinuous decrease below the physiological pH. The cells appear to show increased anion permeability, leading to irreversible damage only under those situations where membrane potentials are expected to be very high. The cells were never found to possess a membrane potential value higher than 200 mV in equilibrium condition, which presumably represents a threshold. A plausible scheme is put forward to depict interplay between the chemiosmotic parameters and ion permeability in *T. ferrooxidans* (Figure 6). A transmembrane potential of 200 mV corresponds to an electrical field strength of about 300,000 V/cm. Such a high field may lead to dielectric breakdown – similar to non-ohmic leak/slip in state 4 mitochondrial respiration[15]. An increased fixed charge on the membrane surface, on the other hand, is also expected to affect membrane organization which in turn may lead to increased permeability. Our preliminary measurements of surface potential by spectroscopic probes suggest that near the physiological pH the surface potential is positive and increasing with decreasing pH[18]. Evaluation of the components of the membrane potential, viz. transmembrane potential and surface potential and their possible relation to the sulphate distribution, thus may lead to further elucidation of the bioenergetics and ion transport mechanisms in this organism.

1. Booth, I. R., *Microbiol. Rev.*, 1985, **45**, 359–378.
2. Matin, A., *FEMS Microbiol. Rev.*, 1990, **75**, 307–318.
3. Mitchell, P., *Physiol. Rev.*, 1966, **41**, 445–502.

4. Cox, J. C., Nicholls, D. G. and Ingledew, W. J., *Biochem. J.*, 1979, **178**, 195–200.
5. Matin, A., Wilson, B., Zychlinsky, E. and Matin, M., *J. Bacteriol.*, 1982, **150**, 582–591.
6. Zychlinsky, E. and Matin, A., *J. Bacteriol.*, 1983, **156**, 1352–1355.
7. Michels, M. and Bakker, E. P., *J. Bacteriol.*, 1985, **161**, 231–237.
8. Goulbourne, E. Jr., Matin, M., Zychlinsky, E. and Matin, A., *J. Bacteriol.*, 1986, **166**, 59–65.
9. Ingledew, W. J., *Biochim. Biophys. Acta*, 1982, **683**, 89–117.
10. Yamanaka, T., Yano, T., Kai, M., Tamegai, H., Sato, A. and Fukumori, Y., in *New Era of Bioenergetics* (ed. Mukohata, Y.), Academic Press, Tokyo, 1991, pp. 223-246.
11. Kar, N. S., Datta, T. K. and Dasgupta, A. K., in Proceedings of the 16th International Congress of Biochemistry and Molecular Biology, New Delhi, Sept. 19–22, 1994, vol. II, p. 427.
12. Silverman, M. P. and Lundgren, D. G., *J. Bacteriol.*, 1959, **77**, 642–647.
13. Rottenberg, H., *Methods Enzymol.*, 1979, **55**, 547–569.
14. Lakowicz, J. R., in *Principles of Fluorescence Spectroscopy*, Plenum Press, New York, 1983.
15. Nicholls, D. G. and Ferguson, S. J., in *Bioenergetics 2*, Academic Press, London, 1992.
16. Cobley, J. G. and Cox, J. C., *Microbiol. Rev.*, 1983, **47**, 579–595.
17. Kraayenhof, R., Sterk, G. J. and Wong Fong Sang, H. W., *Biochemistry*, 1993, **32**, 10057–10066.
18. Kar, N. S. and Dasgupta, A. K., *Indian J. Biochem. Biophys.*, 1996, **33**, 398–402.
19. Alexander, B., Leach, S. and Ingledew, W. J., *J. Gen. Microbiol.*, 1987, **133**, 1171–1179.
20. Takeudi, T.L. and Suzuki, I., *J. Bacteriol.*, 1994, **176**, 913–916.

ACKNOWLEDGMENTS. This work is partly supported by CSIR Research Grant no. 37(0878)/95/EMR-II. NSK is supported by University Research Scheme, University of Kalyani. We thank Prof. C. K. Dasgupta, Dept of Biophysics, Molecular Biology and Genetics, Calcutta University, and Dr D. Mukherjee, Dept of Zoology, University of Kalyani for facilities. The strain ATCC 23270 was kindly provided by Dr P. C. Banerjee, Indian Institute of Chemical Biology, Calcutta.

Received 19 August 1996; revised accepted 22 November 1996.

Visualization in biodiversity research: A case study of Mehao Wildlife Sanctuary, Arunachal Pradesh, north-east India

S. Narendra Prasad, B. Prabakaran* and C. Jeganathan**

Sálim Ali Centre for Ornithology and Natural History, Kalampalayam, Coimbatore 641 010, India
*Regional Remote Sensing Service Centre, Dehara Dun 248 001, India
**Indian Institute of Remote Sensing, Dehra Dun 248 001, India

Biodiversity visualization is a process by which diverse data sources varying from cover types, habitats to species inventories are integrated into a single computer environment. The integration affords a far better degree of spatial reasoning and understanding of biodiversity issues than hitherto attended to. We attempt here to integrate satellite data, digital elevation models derived from the toposheets, slope, aspect, elevation data and known information on some elements of biodiversity. The visualization tools were applied for a case study in Mehao Wildlife Sanctuary, north-east India, a global hotspot of biodiversity. The thematic features included in the visualization are habitats classified using the Landsat thematic mapper (TM) data, plant succession, hotspots of plant diversity, pheasant and takin habitat. The results were 'field tested' for acceptance among the user community. It is concluded that the visualization has a substantial role in furthering biodiversity conservation.

SCIENTIFIC visualization is defined as 'the study, development and use of graphic representation and supporting techniques that facilitate visual communication of knowledge'[1]. The major objective of scientific visualization techniques is to process digital images to produce a simulated model leading to enhanced information content in the images[2]. Biodiversity visualization is a means to achieve cognizance of spatial observations of biological diversity at many scales. This is usually achieved using computer-based scientific data visualization tools[2]. Data visualization tools range from simple statistical bar charts to totally-animated realistic visual simulation and are intended to assist in the data-to-environment translation process. While this process of translating different states of environment into data and statistics exist, the converse of translating data to environmental images is less developed and often neglected[3]. The term biodiversity visualization denotes integration of diverse data sources on biological diversity – ranging from cover types, habitats, species inventories, birds and mammal vocalizations and so on into a single computer environment[3]. In the context of biodiversity research, the chief goal for data visualization lies in achieving accurate and verifiable representation of existing and projected environmental scenarios[2]. The rationale for pursuing visualization is that it aids the scientist with better tools to grapple with the complex issues on patterns of distributions of species, ecosystems and landscape. The manager and policy makers likewise can readily comprehend the issues for day-to-day management. In this paper, we present a case study of data visualization in biodiversity research in north-eastern India, a globally recognized hotspot of biodiversity. The goal is to demonstrate use and integration of digital satellite data, digital elevation models, spatial terrain analyses such as slope, aspect and known information/data on vegetation, mammals and birds. We dem-